HIGH RESOLUTION COMPUTED TOMOGRAPHY OF DAMAGE IN LAMINATED COMPOSITES

Andrew Moffat[1], Peter Wright[1], Jean-Yves Buffière[2], Ian Sinclair[1], Mark Spearing[1]

[1]School of Engineering Sciences, University of Southampton, Hants, SO17 1BJ, UK.
MATEIS, INSA de Lyon, Université de Lyon, Lyon, France.

ABSTRACT

Damage in carbon fibre-epoxy $[90/0]_s$ laminates was investigated using *in situ* synchrotron radiation computed tomography. Using this technique it was possible to observe, in three dimensions, the micromechanisms of damage due to tensile loading. Both inter- and intralaminar damage was observed. Bridging was seen in both the 0˚ splits and transverse ply cracks with the bridging points forming in resin-rich regions in the plies. In the 0˚ splits crack pinning occured in the resin-rich regions but this was not observed in the transverse ply cracks. Several transverse ply cracks may form in a single ply, however crack shielding was observed to inhibit the growth of transverse ply cracks, within close proximity, through the samples. Debonded toughening particles and fibres were associated with the initial stages of delamination.

1. INTRODUCTION

With the increased use of composite materials in primary structures in the next generation of aircraft (e.g. Airbus A350 and Boeing 787) accurate strength and lifing models are increasingly important. Many models have been developed, which aim to predict damage growth, strength and life of fibre reinforced polymer composites [1, 2]. A review of the predictive capabilities of a selection of models carried out by Soden *et al.* [3] showed that the extent of variability between model predictions can be vast. Two likely explanations for the large discrepancy between model outputs are the difficulty in defining an agreed, precise criterion under which failure is considered to have occurred, and the lack of consistency with regard to damage interaction and growth.

Previous work on $[90/0]_s$ carbon fibre-epoxy laminates [4,5] demonstrated that damage can be broadly separated into three different types: intralaminar cracks (including 0˚ splits and transverse ply cracks), interlaminar cracks (delaminations) and fibre breaks. However, this previous work used two-dimensional (2D) imaging and relied on destructive post-failure analysis techniques to interpret the results, and so there is an ambiguity associated with these observations. More recently, advanced experimental techniques have been used to investigate damage growth and the development of strains [6-10] around damage in composite materials but none of these techniques allow for direct observation of the micromechanisms of damage in three dimensions.

X-ray computed tomography (CT) is a well-established technique in medical imaging for producing non-invasive, three-dimensional (3D) images of surface or deep structures within the body. The technique is being increasingly utilised in the field of material science for microstructural characterisation [12,13] and has more recently been used for the evaluation of the micromechanisms of damage [14,15]. X-ray CT is achieved by collecting a series of radiographs at different angles, relative to the sample (see Figure

1). The radiographs are typically reconstructed using a filtered back projection algorithm [16] to generate a representative 3D volume dataset. CT has been used previously to assess damage in composite materials [17,18] but has not been combined with *in situ* loading to observe damage evolution in composite laminates. The work described in this paper aims to clarify the failure mechanisms in $[90/0]_s$ carbon fibre-epoxy samples through *in situ* three dimensional imaging of samples in uni-axial tension using high resolution synchrotron radiation computed tomography (SRCT).

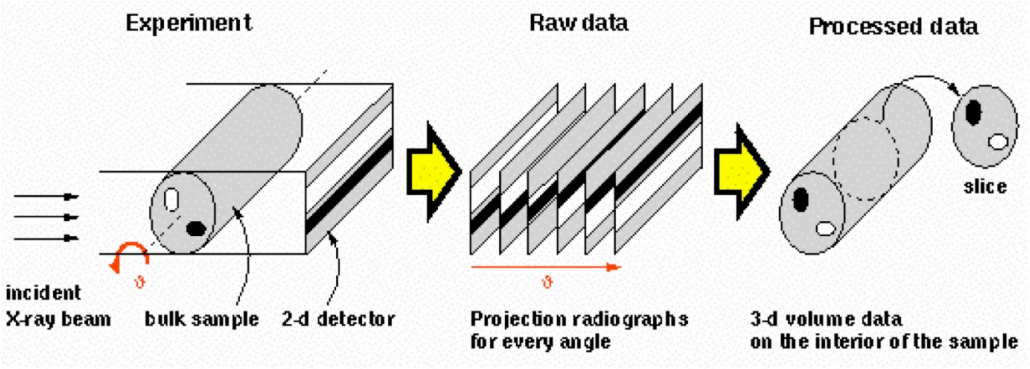

Figure 1: Schematic of the computed tomography process, after [11].

2. MATERIALS

The material used was a commercial pre-preg carbon fibre-epoxy, unidirectional composite. Each ply was 250 μm thick and the laminate used for experiments comprised a $[90/0]_s$ lay-up. The laminate was made into 300 mm^2 sheets which underwent the manufacturers standard consolidation process: a pressure of 1 bar under vacuum and 7 bar in an autoclave, heat-up at 2˚C/min to 180˚C and a held for 120 minutes, and finally cooled at 4˚C/min to room temperature. 4 mm wide specimens with symmetric 1 mm edge notches were machined using an abrasive water jet. The samples were adhesively bonded to aluminium tabs to allow loading. Several samples were tested to failure and a mean failure stress of 960 MPa was recorded.

3. EXPERIMENTAL METHODS

In situ uni-axial tensile tests, monitored by X-ray tomography, were performed at the European Synchrotron Radiation Facility (ESRF) on beamline ID19. This provides a monochromatic and highly coherent X-ray beam, and was used at an energy of 20 keV for this work. Imaging conditions where set for both absorption and phase contrast (edge-detection regime) [19]. The samples were loaded in a specially designed rig attached to a precision movement stage. The samples were placed 37 mm from a 14 bit fast read-out, low noise (FReLoN) detector attached to a 2048^2 CCD camera. An isotropic voxel size of 1.4 μm^3 was achieved using this system. During each tomographic scan 1000 radiographs were collected at regular increments over 180˚ rotation. The exposure time for each radiograph was 50 ms, which resulted in scan times of less than 4 minutes. The radiographs were reconstructed using ESRF in-house software and the resulting 3D volumes were analysed using commercially available software. To monitor crack evolution samples were imaged at increasing stresses from 30-60 $\%\sigma_f$. Several samples were also loaded to a single stress and scanned in the loaded and unloaded state.

4. RESULTS

4.1 Intralaminar damage

The differences in X-ray attenuation and refractive index enable the identification of the individual constituents of a volume scanned using X-ray CT, in this case: fibres, matrix and damage, by their greyscale values. It is therefore possible to segment the damage from the surrounding material, revealing its 3D shape. This has been performed in Figure 2 to reveal interlaminar damage at 40% σ_f. The surrounding material has been partially withdrawn to a position near the interface of the 0˚ plies. Both the 0˚ splits and transverse ply cracks (in the outer 90˚ ply) have been identified. Whilst the general direction of fibres in the 0˚ ply is in the y direction, some fibre misalignment can be observed. The notches have a rough appearance because of the abrasive water jet used in the manufacturing process, however all samples were scanned prior to loading showing that no significant damage had been generated in the material by the cutting process.

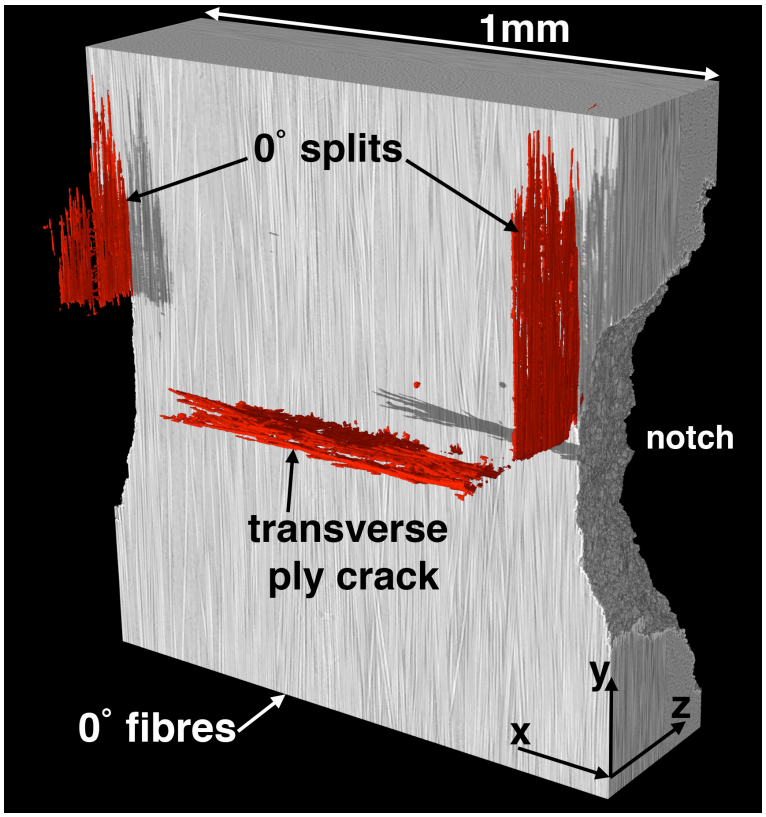

Figure 2: Tomography image of intralaminar damage in a $[90,0]_s$ laminate. The bulk of the composite has been withdrawn to reveal the damage in red.

Experimental observations indicate that intralaminar damage can initiate at stresses less than 30% σ_f in notched samples, but it was not possible to determine if one type of damage initiated before the other from these tests. It can be seen in Figure 2 that the intralaminar cracks follow the direction of the ply in which they form. In Figure 2 the 0˚ splits have only initiated above the notch. This was not a consistent observation in all the samples investigated, with splits forming on either side of the notch. In Figure 2 the transverse ply crack initiated from the right hand notch, at this stress the crack had not propagated completely through the width of the sample. In both types of intralaminar

damage the crack front is non-planar with regions of advanced and retarded crack growth.

Analysis of the 0˚ plies using CT sectioning reveals that there are regions where the fibres are closely packed, and also resin-rich regions. The resin-rich regions occur between the plies and also in the centre of each ply; this is due to the method used to manufacture the pre-preg material. The appearance of the cracks in the resin-rich regions is different to that in the close packed fibre regions. Cracks in the resin-rich regions are comprised of many smaller echelon cracks, which form at 45˚ to the loading direction; these have been identified in Figure 3. Damage in the close packed fibre regions has a smoother form and appears to be initiated by decohesion of the fibre/matrix interface.

If the resin-rich regions are more closely examined it is be seen that they contain roughly spherical particles; these are identified in Figure 3(a). Early CFRP composites had low impact toughness and so to improve this property toughening particles are added [20]. There are several types of toughening particles, for example liquid rubbers [21], functionally terminated thermoplastics [22], and polyorganic siloxane [23]. Whilst the chemistry of the toughening particles is different, the modifiers used to produce them have similar characteristics: they are usually soluble in the epoxy and precipitate out of the epoxy before gelation.

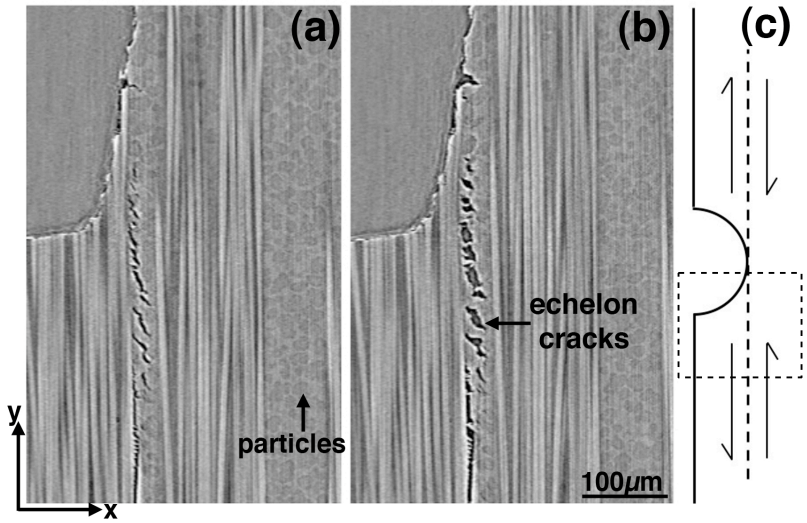

Figure 3: CT section of a sample at (a) zero load (after prior loading to 50%σ_f), (b) 50%σ_f showing echelon cracks shearing and (c) schematic illustration of overall sense of shear displacements occurring under load. The particle toughened resin-rich region may also be observed.

Two types of echelon cracks form in the resin-rich regions. The first type are ~20μm in length and are associated with the toughening particles in the matrix phase. Whilst the toughening particles have been observed to debond completely from the matrix under loading, it is more usual for the particles to be partially debonded on one side and this may be seen in Figure 3(a). The second type are smaller in size (~5μm), these may be seen towards the bottom of the split. They are not associated with the toughening particles and are usually seen emanating from the edge of fibres into the resin-rich

regions. Figures 3(a) and (b) show the same CT section (in the *xy* plane) through a sample scanned in the unloaded and loaded (50% σ_f) states respectively. In the unloaded state the damage is visible; the echelon cracks are open due to local residual stresses. In the loaded state the echelon cracks have a grater level of opening. It is also possible to see that in the loaded state the cracks have sheared, indicating that a Mode II displacement is associated with 0˚ splits, as illustrated in Figure 3(c).

The material between the echelon cracks, which consists of both epoxy and toughening particles, provide bridging points [24] across the split. The 0˚ splits were observed to be consistently retarded or pinned in the resin-rich regions. The splits initiated at a higher stress in the resin-rich regions so that 'forks' of crack growth propagated away from the notch (in the closed packed fibre regions) before the split had initiated in the resin-rich region. The enhanced resistance to crack growth may be largely attributed to the increased ductility of the matrix, which results from the high volume fraction of toughening particles. This reduces the compliance of the matrix and so effects the load transferred from the matrix, effectively reducing the matrix stress [25]. The bridging points will also act as a traction on crack opening and so are likely to reduce the crack driving force of the 0˚ splits.

Resin-rich regions are also apparent in the centre of the 90˚ plies. The appearance of damage in these resin-rich regions was similar to that in the 0˚ splits, i.e. bridged or ligamented cracks that form at 45˚ to the loading direction. However, there was a greater connectivity between the cracks and so fewer bridging points between the crack flanks *cf.* the echelon cracks in the 0˚ plies. Whilst the transverse ply crack fronts are irregular they are not severely retarded in the resin-rich regions in the same way as in the 0˚ splits. The lower number of bridging points may be attributed to loading in the 90˚ plies. The mode of loading is primarily Mode I and because of the orientation of the fibres they bear a lower proportion of the load, which results in higher matrix stresses in the 90˚ plies compared with that in the 0˚ plies. When transverse ply cracks form, the displacements associated with the damage (for example: crack opening displacement) are therefore greater in the transverse ply cracks causing the toughening particles to experience larger strains (and therefore stresses) resulting in an increased level of failure and therefore fewer bridging points. It is of interest to note that misaligned fibres were also a source of bridging in transverse ply cracks, although these occurred infrequently.

Several transverse ply cracks can form in each 90˚ ply. Capturing the evolution of transverse ply cracks was difficult because it was usual for them to propagate through the sample within the 10% σ_f intervals at which tomographic imaging was performed. However, it was observed that when two transverse ply cracks are within close proximity a complicated stress state can of course develop due to the unloaded material above and below the cracks, which may then cause shielding at their tips. An example of shielding is presented in Figure 4: (a) shows a sample loaded to 40% σ_f and (b) shows the same sample loaded to 50% σ_f. There are two transverse ply cracks, which each initiated at the notches on either side of the sample. At 40% σ_f the crack tips are at approximately the same *x* position in the sample. After increasing the load to 50% σ_f both cracks have grown (in particular the upper crack) but neither has breached the side of the sample. Although not shown in Figure 4, upon further loading to 60% σ_f neither

crack propagated entirely through the sample. To quantify the extent of shielding and other mechanisms future investigations will use fiducial markers in the bulk of the sample to determine full-field strain maps. Such information will clearly be of use in model development and validation.

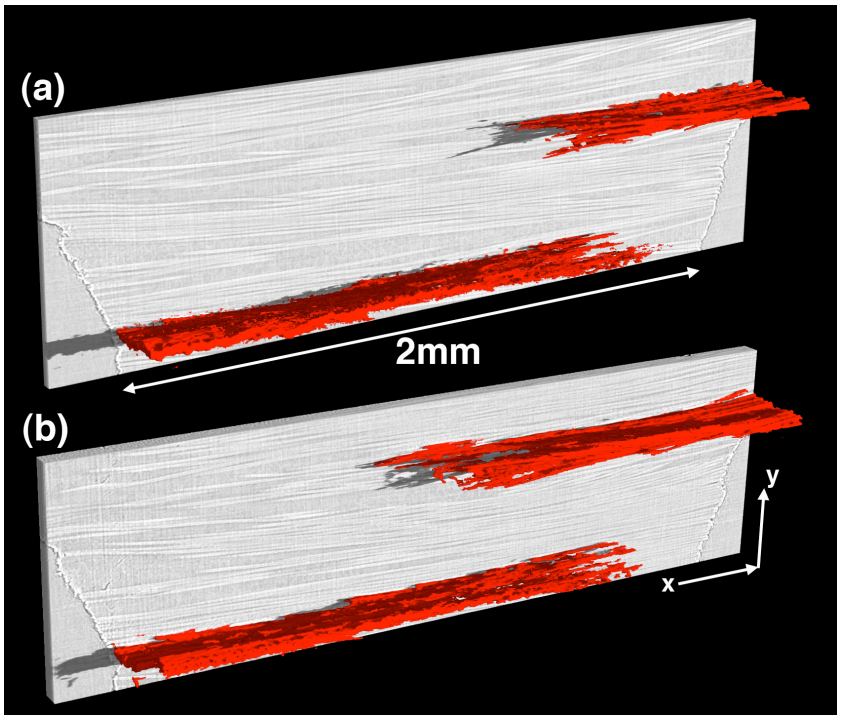

Figure 4: Transverse ply cracks shielding each other in a sample loaded to (a) 40%σ_f and (b) 50%σ_f.

4.2 Interlaminar damage

It is well established that because of differences in load transfer in the 0˚ and 90˚ plies, a stress gradient exists over the interlaminar region. The stress distribution in the interlaminar region is made more complex when intralaminar damage forms; for example: the shear displacements associated with 0˚ splits (the effect of which was shown in Figure 3) must be accommodated in the interlaminar regions. The results of this study indicate that at global stress of 40% σ_f or lower the amount of damage in the interlaminar region is minimal. The interlaminar regions are resin-rich and so contain a high volume fraction of toughening particles. The displacements are therefore accommodated by the deformation of the toughened (and therefore ductile) layer.

At a global stress of 50% σ_f the onset of delamination was observed, this takes the form of micro-damage sites; examples of these are presented in Figure 5. These sites initially form in close proximity to the intralaminar damage. Both Figure 5(a) and (b) are CT sections through the resin-rich interlaminar region in the *xy* plane, toughening particles and stray fibres can be seen in these figures. In (a) the edge of the transverse ply crack has been identified and, like other damage in the resin-rich regions, is comprised of a complex array of micro-cracks at 45˚ to the loading direction. Below the transverse ply crack the small micro-damage regions associated with toughening particles, that are partially debonded from the epoxy matrix, can be seen. This damage is characteristic of that located around transverse ply cracks in this material. The micro-damage in the

interlaminar regions located around the 0˚ splits is primarily associated with partially debonded fibres; this can be seen in Figure 5(b). Figure 5(b) shows the confluence of a transverse ply crack and a 0˚ split. The debonded fibres form a crosshatched pattern. Close to the transverse ply crack some debonded toughening particles may also be observed. Figure 5(b) is a 2D section, an advantage of the tomography technique is that the data is three-dimensional and it is possible to see either side of this slice. Figure 5(c) is a 3D image of the interlaminar damage shown in (b). The damage has been segmented from the surrounding material, to reveal the characteristic crosshatched pattern. With an increase in the applied stress further micro-damage sites form and the micro-damage propagates and coalesces to eventually form large-scale delamination.

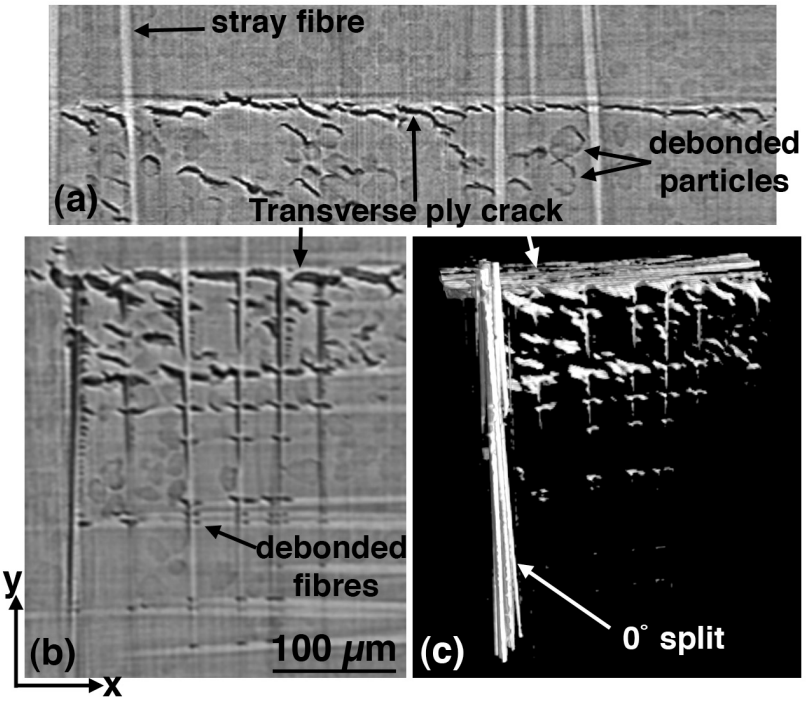

Figure 5: The early stages of delamination: (a) shows damage at toughening particles in the interlaminar region below a transverse ply crack, (b) shows damage at fibres and toughening particles at the confluence of a transverse ply crack and a 0˚ split, and (c) is a 3D image of (b).

5. CONCLUSIONS

SRCT has been used to monitor damage in carbon fibre-epoxy laminates at applied stresses between 30%-60% σ_f and several complex micromechanisms have been observed. Intralaminar damage was seen to initiate below 30% σ_f with damage in the interlaminar regions occur after 40% σ_f to accommodate the strains associated with intralaminar damage. In the resin-rich regions of the 0˚ splits, echelon cracks form at 45˚ to the applied load, whilst in the close-packed fibre regions damage has a smoother appearance and appears to be via the debonding of the fibre-matrix interface. Micro-cracks aligned at 45˚ to the tensile direction also occur in the resin-rich regions of the transverse ply cracks. However, compared with the 0˚ splits there is a lower level of bridging and crack retardation/pinning. Crack shielding of two cracks located within 2 ply widths of each other was seen in transverse ply cracks. The onset of delamination was observed: micro-damage initiates via the debonding of toughening particles and

fibres debonding from the epoxy matrix. Future work will concentrate on using fiducual markers in the bulk of the composite to obtain full-field strain maps for composite materials under static and fatigue loads.

ACKNOWLEDGEMENTS
The authors acknowledge: the European Synchrotron Radiation Facility for provision of synchrotron radiation facilities and would like to thank Greg Johnson for assistance in using beamline ID19, Airbus for supplying materials and EPSRC, grant EP/E003427/1, for funding. SMS holds a Royal Society Wolfson Research Merit Award.

REFERENCES
1. Barbero, E.J., G.F. Abdelal, and A. Caceres, "A micromechanics approach for damage modelling of polymer matrix composites". *Composite Structures*, 2005;67(4): p. 427-436.
2. Maimi, P., Camanho, P.P., Mayugo, J.A., Davila, C.G., "A continuum damage model for composite laminates: Part I - constitutive model". *Mechanics of Materials*, 2007;39(10): p. 897-908.
3. Soden, P.D., M.J. Hinton, and A.S. Kaddour, "A comparison of the predictive capabilities of current failure theories for composite laminates". *Composite Science and Technology*, 1998;58(7): p. 1255-1254.
4. Spearing, S.M. and P.W.R. Beaumont, "Fatigue damage mechanics of composite materials. I. Experimental measurement of damage and post-fatigue properties". *Composites Science and Technology,* 1992;44(2): p. 159-68.
5. Kortschot, M.T. and P.W.R. Beaumont, "Damage mechanics of composite materials. I. Measurements of damage and strength". *Composites Science and Technology*, 1990;39(4): p. 289-301.
6. Dzenis, Y.A. and J. Qian, "Analysis of microdamage evolution histories in composites". *International Journal of Solids and Structures*, 2001;38(10-13): p. 1831-1854.
7. Sihn, S., Kim, R.Y., Kawabe, K., Tsai, S.W., "Experimental studies of thin-ply laminated composites". *Composites Science and Technology*, 2007;67(6): p. 996-1008.
8. Yashiro, S., T. Okabe, and N. Takeda, "Damage identification in a holed CFRP laminate using a chirped fiber Bragg grating sensor". *Composites Science and Technology*, 2007;67(2): p. 286-295.
9. Emery, T.R. and J.M. Dulieu-Barton, "Damage monitoring of composite materials using pulsed phase thermography and thermoelastic stress analysis". *Key Engineering Materials*, 2007;347: p. 621-626.
10. Pierron, F., Green, B., Wisnom, M.R., Hallett, S.R., "Full-field assessment of the damage process of laminated composite open-hole tensile specimens. Part II: Experimental results". *Composites Part A: Applied Science and Manufacturing*, 2007;38(11): p. 2321-2332.
11. ESRF, Principles of computerized tomography, 2007; http://www.esrf.eu.
12. Moffat, A.J., Mellor, B.G., Sinclair, I., Reed, P.A.S., "The mechanisms of long fatigue crack growth behaviour in Al-Si casting alloys at room and elevated temperature". *Materials Science and Technology*, 2007;23(12): p. 1396-1401.
13. Salvo, L., Cloetens, P., Maire, E., Zabler, S., Blandin, J.J., Buffière, J-Y, Ludwig, W., Boller, E., Bellet, D., Josserond, C., "X-ray micro-tomography an

attractive characterisation technique in materials science". *Nuclear Instruments and Methods in Physics Research Section B: Beam Interactions with Materials and Atoms*, 2003;200: p. 273-286.
14. Khor, K.H., Buffière, J-Y., Ludwig, W., Toda, H., Ubhi, H.S., Gregson, P.J., Sinclair, I., "In situ high resolution synchrotron x-ray tomography of fatigue crack closure micromechanisms". *Journal of Physics Condensed Matter*, 2004;16(33): p. 3511-3515.
15. Ferrie, E., Buffière, J-Y., Ludwig, W., Gravouil, A., Edwards, L., "Fatigue crack propagation: In situ visualization using X-ray microtomography and 3D simulation using the extended finite element method". *Acta Materialia*, 2006;54(4): p. 1111-1122.
16. Kak, A. and M. Slaney, "Principles of computerized tomographic imaging". 1988, New York, USA: IEEE press.
17. Aroush, D.R.-B., Maire, E., Gauthier, C., Youssef, S., Cloetens, P., Wagner, H.D., "A study of fracture of unidirectional composites using in situ high-resolution synchrotron X-ray microtomography". *Composites Science and Technology*, 2006;66(10): p. 1348-1353.
18. Schilling, P.J., Karedla, B.R., Tatiparthi, A.K., Verges, M.A., Herrington, P.D., "X-ray computed microtomography of internal damage in fiber reinforced polymer matrix composites". *Composites Science and Technology*, 2005;65(14): p. 2071-2078.
19. Cloetens, P., Boller, E., Ludwig, W., Baruchel, J., Schlenker, M., "Absorption and phase contrast imaging with synchrotron radiation". *Europhysics News*, 2001;32(2).
20 Scott, J.M., Phillips, D.C., "Carbon fibre composites with rubber toughened matrices". *Journal of Materials Science*, 1975;10 (4): p. 551-562.
21 McGarry, F.J., "Building Design with Fibre Reinforced Materials". *Proceeding of the Royal Society of London, Series A*, 1970;319 (1536): p. 59-68.
22 Bucknall, C.B., Partridge, I.K., "Phase separation in epoxy resins containing polyethersulphone". *Polymer*, 1983;24 (5): p. 639-644.
23 Yorkgitis, F.M., Tran, C., Eiss, N.S., Hu, T.Y., Yilgor, I., Wilkes, G.L., McGrath, J.E., "Siloxane modifiers for epoxy resins". *Advances in Chemistry Series*, Washington, 1984, p. 137-161.
24. Kunz-Douglass, S., Beaumont, P.W.R., Ashby, M.F., "A model for the toughness of epoxy-rubber particulate composites". *Journal of Materials Science*, 1980;15(5): p. 1109-23.
25. Clyne, T.W. Withers, P.J., "An Introduction to metal matrix composites". Cambridge Solid State Science Series. 1993, Cambridge University Press, UK.